applied optics

Passive Q-switching of a Tm,Ho:KLu(WO$_4$)$_2$ microchip laser by a Cr:ZnS saturable absorber

J. M. Serres,[1] P. Loiko,[1,2] X. Mateos,[1,3,5,*] V. Jambunathan,[4] A. S. Yasukevich,[2] K. V. Yumashev,[2] V. Petrov,[3] U. Griebner,[3] M. Aguiló,[1] and F. Díaz[1]

[1]Física i Cristal·lografia de Materials i Nanomaterials (FiCMA-FiCNA), Universitat Rovira i Virgili (URV), Campus Sescelades, c/Marcel·lí Domingo, s/n., Tarragona E-43007, Spain
[2]Center for Optical Materials and Technologies (COMT), Belarusian National Technical University, 65/17 Nezavisimosti Ave., Minsk 220013, Belarus
[3]Max Born Institute for Nonlinear Optics and Short Pulse Spectroscopy, 2A Max-Born-Str., Berlin D-12489, Germany
[4]HiLASE Centre, Institute of Physics ASCR, Za Radnicí 828, Dolní Břežany 25241, Czech Republic
[5]e-mail: mateos@mbi-berlin.de
*Corresponding author: xavier.mateos@urv.cat

Received 4 March 2016; revised 6 April 2016; accepted 6 April 2016; posted 7 April 2016 (Doc. ID 260487); published 3 May 2016

A diode-pumped Tm,Ho:KLu(WO$_4$)$_2$ microchip laser passively *Q*-switched with a Cr:ZnS saturable absorber generated an average output power of 131 mW at 2063.6 nm with a slope efficiency of 11% and a *Q*-switching conversion efficiency of 58%. The pulse characteristics were 14 ns/9 μJ at a pulse repetition frequency of 14.5 kHz. With higher modulation depth of the saturable absorber, 9 ns/10.4 μJ/8.2 kHz pulses were generated at 2061.1 nm, corresponding to a record peak power extracted from a passively *Q*-switched Tm,Ho laser of 1.15 kW. A theoretical model is presented, predicting the pulse energy and duration. The simulations are in good agreement with the experimental results.

OCIS codes: (140.3070) Infrared and far-infrared lasers; (140.3540) Lasers, Q-switched; (140.3380) Laser materials.

http://dx.doi.org/10.1364/AO.55.003757

1. INTRODUCTION

The holmium (Ho^{3+}) ion is attractive for lasing due its wavelength-tunable emission at ~2 μm ($^5I_7 \rightarrow {}^5I_8$ transition). Such an emission is eye-safe and of practical interest for remote sensing, metrology, and medical applications. Holmium lasers are also used for pumping mid-IR optical parametric oscillators [1]. An usual scheme to excite Ho^{3+} is the energy transfer (ET) from Thulium (Tm^{3+}) ions, $^3F_4(Tm^{3+}) \rightarrow {}^5I_7(Ho^{3+})$ by co-doping the host material [2]. This approach has the advantage of enhanced pump efficiency because the Tm^{3+} ions strongly absorb the emission of commercial AlGaAs laser diodes at ~0.8 μm. The ET in the Tm^{3+}, Ho^{3+} pair is very efficient even at low Ho^{3+} concentrations, achieved by efficient cross relaxation between the Tm^{3+} ions at high concentration whereas the Ho^{3+} ions act as efficient traps [3]. Consequently, an optimum codoping ratio (N_{Ho}:N_{Tm}, from 1:5 to 1:10) exists providing both high Tm^{3+} absorption and weak upconversion.

Tm,Ho codoped materials are very suitable for the development of compact diode-pumped laser sources at ~2 μm [4–6]. This is especially true by exploiting the microchip laser concept [7] with a gain material placed in a plano–plano cavity without air gaps. Such a compact, robust, and misalignment-free design provides low intracavity losses and high laser efficiency. Continuous wave (CW) Tm,Ho microchip lasers were realized with a number of hosts such as $LiYF_4$, $YAlO_3$, YVO_4, and $GdVO_4$ [8–12]. Recently, we studied potassium lutetium double tungstate, $KLu(WO_4)_2$ or KLuW for short, which has proved to be very suitable host for rare earth doping [13]. This finding holds also for Tm,Ho doping because it provides high absorption and emission cross sections together with high ET efficiency [14]. A room-temperature CW Tm,Ho:KLuW microchip laser generated 451 mW at 2081 nm with a slope efficiency of 31% [15].

Passively *Q*-switched (PQS) microchip lasers containing a saturable absorber (SA) in the cavity [16] may generate very short pulses due to the reduced cavity round-trip time [17]. The stabilization of the laser mode in the microchip laser cavity is typically ensured by a positive thermal lens of the gain material [18]. The effect of the thermal lens also strongly focused the laser mode in the SA resulting in its easy bleaching. Thus, PQS microchip lasers are also attractive for the generation of high peak powers. We are aware of only one report on a PQS Tm,Ho microchip laser [19]. However, due to one particular limitation of the SA used in [19] (single-layer graphene), namely, the low modulation depth, this laser generated 200 ns/0.2 μJ pulses with a peak power of only ~1 W. Several previous studies were devoted to PQS Tm,Ho bulk lasers using $LiYF_4$, $LiLuF_4$, $YAlO_3$, and YVO_4 host crystals and Cr^{2+}:ZnS or

carbon nanostructures as SAs [20–23]. However, in such lasers, the typical pulse durations were still a few hundred nanoseconds (ns) and the peak power did not exceed a few tens of watts (W).

In this paper, the first Tm,Ho microchip laser PQS with a Cr^{2+}:ZnS SA is presented. Using a Tm,Ho:KLuW crystal as gain medium, peak powers exceeding the kilowatt level are achieved. Recently, Cr^{2+}:ZnS has been successfully applied for Q-switching of bulk [24] and microchip [25] Tm:KLuW lasers which operate at shorter wavelengths.

2. EXPERIMENT

The studied crystal with composition 5.0 at. % Tm, 0.5 at. % Ho:$KLu(WO_4)_2$ or Tm,Ho:KLuW for short was grown by the top-seeded solution growth slow-cooling method and potassium ditungstate $K_2W_2O_7$ was used as a solvent; details about the growth procedure can be found in [13]. The starting materials were K_2CO_3, WO_3, and Ln_2O_3 (Ln = Lu, Tm and Ho) with 99.99% purity. The actual ion densities in the crystal measured by electron probe microanalysis were $N_{Tm} = 2.30 \times 10^{20}$ at/cm^3 and $N_{Ho} = 0.53 \times 10^{20}$ at/cm^3. Such doping levels for Tm^{3+} and Ho^{3+} ions provided high prevalence of direct $Tm^{3+} \rightarrow Ho^{3+}$ energy transfer over the reverse $Ho^{3+} \rightarrow Tm^{3+}$ process [19] (expressed by an equilibrium constant, $\theta = 0.089$) which prevented unwanted colasing of both ions [26]. The latter, in turn, could be the main limitation for a stable Q-switched operation with this crystal.

A rectangular sample was cut from the as-grown bulk in the frame of the dielectric axes with dimensions 2.86(g) mm × 2.86(m) mm × 2.94(p) mm. It was oriented for light propagation along the N_g-axis. This crystal orientation was selected because it provides a positive thermal lens [15,27] required for stabilization of the laser mode in a plano–plano microchip cavity. Both $m \times p$ crystal faces were polished to laser quality and remained uncoated. The crystal was mounted in a water-cooled copper holder (kept at 14°C) and cooled from all four side faces. Indium foil was used to improve thermal contact.

The laser cavity consisted of a plane pump mirror that was AR-coated for 0.7–1 μm and HR-coated for 1.8–2.1 μm and a plane output coupler (OC) providing a transmission of $T_{OC} = 5\%$ at the laser wavelength. The choice of this OC will be explained below. Two commercial SAs from polycrystalline Cr^{2+}:ZnS with thicknesses of 2.18 and 2.21 mm were studied (IPG Photonics). The SAs were AR-coated for the 1.8–2.2 μm range. The initial transmission at the laser wavelength, T_{SA}, was 89% and 90.5%, respectively. Small-signal transmission of both SAs at ~2.2 μm (i.e., outside of the Cr^{2+} ions absorption band) was 92.5%, representing 7.5% single-pass nonsaturable loss. It is attributed to strong scattering and imperfect optical quality of this polycrystalline material and partially to residual Fresnel loss due to imperfect coating. Thus, the saturable absorption α'_{SA} was 3.5% and 2%, respectively. The passively cooled SAs were placed between the crystal and the OC and. The cavity contained no air gaps, and its total length was ~5.06 mm.

The crystal was pumped by a fiber-coupled AlGaAs laser diode (N.A. = 0.22, fiber core diameter: 200 μm) operating at $\lambda_p = 805$ nm (excitation wavelength for the $^3H_6 \rightarrow {}^3H_4$ transition of Tm^{3+}). The unpolarized output from the diode was reimaged into the crystal by a lens assembly (1∶1 image ratio, focal length: 30 mm) resulting in a pump spot radius $w_p = 100$ μm. The M^2 parameter for the pump beam, estimated from the relation $w_p \times$ N.A. $= (\lambda_p/\pi) \times M^2$, amounted to ~86. Thus, the confocal parameter for the pump beam $2z_R = 2\pi w_p^2 n/(\lambda_p M^2) = 1.8$ mm. The absorption of the pump radiation in the crystal was 60%. The radius of the laser mode in the crystal and SA was calculated with the ABCD-method for the "hot" cavity to be $w_l = 60 \pm 5$ μm. The thermal lens was described as a thin astigmatic lens. For the pumped crystal, the following parameters of the thermal lens were used: $M = 24.9$ and 24.1 m^{-1}/W for the mg- and pg-principal meridional planes, respectively [15]. Here, $M = dD/dP_{abs}$ is the so-called sensitivity factor of the thermal lens, P_{abs} is the absorbed pump power, $D = 1/f$ is the optical (refractive) power of the lens, and f is its focal length [28]. Thus, for the maximum studied P_{abs} of 1.9 W, $f = 21$ and 22 mm for the mg- and pg-planes, respectively.

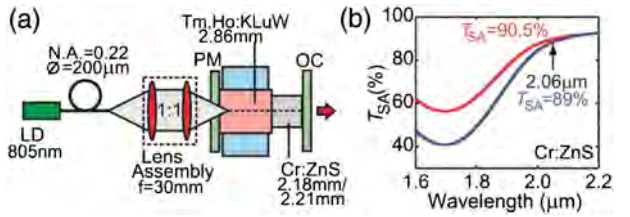

Fig. 1. (a) Scheme of the passively Q-switched Tm,Ho:KLuW microchip laser. LD, laser diode; PM, pump mirror; OC, output coupler. (b) Transmission spectra of the used Cr:ZnS SAs.

The scheme for the PQS Tm,Ho:KLuW microchip laser is shown in Fig. 1(a). The transmission spectra of the used Cr:ZnS SAs are shown in Fig. 1(b). A fast InGaAs photodiode (rise time: 200 ps) and 2 GHz digital oscilloscope (Tektronix DPO5204B) were used for detection of the Q-switched pulses.

3. MODEL OF A Q-SWITCHED LASER

First we modeled the pulse energy and pulse duration for the PQS Tm,Ho:KLuW microchip laser. This model is an adaptation of that presented in [29] for a Yb microchip laser. We consider a quasi-three-level laser system. PQS is realized by a "slow" SA, i.e., a SA with a recovery time much longer than the pulse duration. We introduce the following variables: (i) $\Phi_g = I_g/h\nu_g$, the photon flux density at the laser frequency (I_g is the laser radiation intensity, h is the Planck constant, and ν_g is the laser frequency), (ii) $N_{2g} = N_2 - \beta_g N_{Ho}$, the effective population of the upper laser level (N_2 is its actual population, $\beta_g = \sigma^g_{abs}/(\sigma^g_{SE} + \sigma^g_{abs})$ is the parameter characterizing the conditions for bleaching of the active medium at the laser frequency, and σ^g_{SE} and σ^g_{abs} are the stimulated-emission and absorption cross sections for the active medium at the laser frequency, respectively), and (iii) N_{gs}, the population of the ground state of the SA. All these variables are averaged over the laser mode volume. For *single-pulse* generation, the system of rate equations is

$$\frac{d\Phi_g}{dt} = \frac{c\mu}{n}(\sigma_g N_{2g} - k_L - k_{SA})\Phi_g, \tag{1a}$$

$$\frac{dN_{2g}}{dt} = -\sigma_g N_{2g}\Phi_g, \tag{1b}$$

$$\frac{dN_{gs}}{dt} = -\xi\sigma_{gs}N_{gs}\Phi_g. \tag{1c}$$

Here, c is the speed of light, $\mu = l_{\mathrm{AM}}n_{\mathrm{AM}}/l_c$ is the resonator filling factor; l_{AM} is the active element length; n_{AM} is the refractive index of the active element; l_c is the optical length of the resonator; $\sigma_g = \sigma^g_{\mathrm{SE}} + \sigma^g_{\mathrm{abs}}$; $k_L = -[\ln(1 - T_{\mathrm{OC}}) + \ln(1 - L)]/(2l_{\mathrm{AM}})$ is the resonator loss coefficient, where L is the coefficient of passive intracavity loss; $k_{\mathrm{SA}} = (\sigma_{gs}N_{gs} + \sigma_{es}N_{es})l_{\mathrm{SA}}/l_{\mathrm{AM}}$ is the loss coefficient in the SA; σ_{gs} and σ_{es} are the ground- and excited-state absorption cross sections for the SA, respectively; N_{es} is the population of the excited state of the SA; l_{SA} is the SA length; and $\xi = A_g/A_{\mathrm{SA}}$ is the ratio of effective areas of the lasing mode in the active medium (A_g) and in the SA (A_{SA}).

The energy (E_{out}) and duration (Δt) of a single pulse are then determined as

$$E_{\mathrm{out}} = V_g k_{\mathrm{act}} h\nu_g \frac{1}{\sigma_g} \ln\left(\frac{N^i_{2\,g}}{N^f_{2g}}\right), \tag{2a}$$

$$\Delta t = E_{\mathrm{out}}/P_{\mathrm{peak}}, \quad \text{where } P_{\mathrm{peak}} = V_g k_{\mathrm{act}} h\nu_g \Phi_g(N^t_{2g}). \tag{2b}$$

Here, $N^i_{2g} = (k_L l_{\mathrm{AM}} - \ln T_{\mathrm{SA}})/(\sigma_g l_{\mathrm{AM}})$ is the initial effective population of the upper laser level, and N^t_{2g} and N^f_{2g} correspond to the moment when Φ_g reaches its maximum value (maximum of the pulse) and to the termination of the laser pulse, respectively. The solutions of Eq. (1) for $\Phi_g(N_{2g})$, N^t_{2g}, and N^f_{2g} parameters are given in Appendix A.

The material parameters of Tm,Ho:KLuW and Cr:ZnS used for calculations [14,19,30] are listed in Table 1.

From the point of view of the laser efficiency, the selection of the OC for the Tm,Ho:KLuW laser is limited by a strong upconversion loss for high T_{OC} [15] due to a high inversion ratio and, hence, high population of the upper laser level of Ho^{3+}. Consequently, low transmittance of the OC and high transmission of the SA are desirable. Considering the latter, we have calculated the pulse duration and energy for the PQS Tm, Ho:KLuW microchip laser for $T_{\mathrm{OC}} = 1\%\ldots9\%$ and $\alpha'_{\mathrm{SA}} = 6\%$, 4%, or 2%, as shown in Fig. 2. The model indicates that with an increase in the modulation depth of the SA, the pulse duration will be shortened from ~13 to 7 ns and there exists an optimum range of T_{OC}, namely, 4%…6% corresponding to the shortest pulses. The pulse energy is expected to increase with the increase in α'_{SA}. Concerning its dependence on the OC transmittance, it is nearly saturated for $T_{\mathrm{OC}} > 4\%$. All these considerations led to the selection of $T_{\mathrm{OC}} = 5\%$ as the one close to optimum for our designed microchip, and a peak power >1 kW is expected.

Table 1. Material Parameters[a] of the Tm,Ho:KLuW Laser Crystal and Cr:ZnS SA Used for the Calculations [14,19,30]

Parameter	Notation	Value
AM: Tm,Ho:KLuW[b]		
Absorption cross section	σ^g_{abs}	0.7×10^{-20} cm^2
Stimulated-emission cross section	σ^g_{SE}	2.4×10^{-20} cm^2
Lifetime of Ho^{3+}ions/Tm^{3+}–Ho^{3+} pair	$\tau_{\mathrm{Ho}}(^5\mathrm{I}_7)/\tau_{\mathrm{Tm-Ho}}$	4.8 ms/2.1 ms
Refractive index	n_{AM}	1.9852
SA:Cr^{2+}:ZnS		
Ground/excited-state absorption cross section	σ_{gs}/σ_{es}	0.1×10^{-18} cm^2/≈0
Saturation fluence	$F_S = h\nu_l/\sigma_{gs}$	1.07 J/cm^2
Recovery time	$\tau(^5E)$	5 μs
Nonsaturable loss		7.5%
Refractive index	n_{SA}	2.2647

[a]At the laser wavelength, $\lambda_l = 2.06$ μm.
[b]For light polarization E‖Nm.

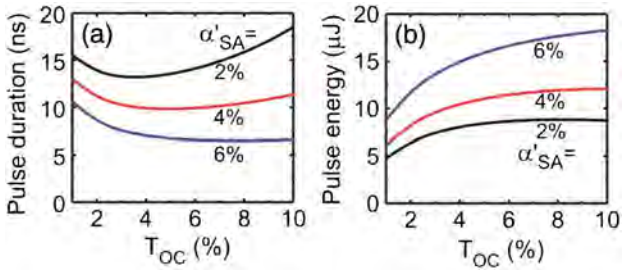

Fig. 2. Modeling of (a) the pulse duration and (b) energy for the Tm,Ho:KLuW microchip laser passively Q-switched by a Cr:ZnS SA. α'_{SA}, modulation depth of the saturable absorber; T_{OC}, transmission of the output coupler.

4. RESULTS AND DISCUSSION

In the CW regime, we achieved 225 mW at ~2063 nm with a slope efficiency $\eta = 16\%$ (with respect to the absorbed pump power); see Fig. 3. The laser threshold was at $P_{\mathrm{abs}} = 0.5$ W, and the optical-to-optical efficiency amounted to 12%. Further power scaling of this laser was limited by strong thermal effects observed at $P_{\mathrm{abs}} > 2$ W, leading to a roll-off of the output power due to a strong upconversion. The output emission from this laser was linearly polarized, $E\|N_m$, naturally selected by the anisotropy of the gain.

Stable Q-switching was achieved for the two studied SAs for $P_{\mathrm{abs}} \le 2$ W. Within this range of absorbed power, the

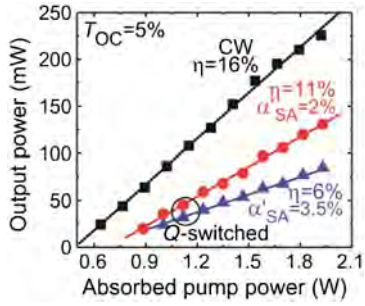

Fig. 3. Output characteristics of CW and passively Q-switched Tm,Ho:KLuW microchip lasers, where $T_{\mathrm{OC}} = 5\%$, and η is the slope efficiency.

input–output dependence of the PQS Tm,Ho:KLuW microchip laser was linear. The laser output was also linearly polarized, $E\|N_m$. The maximum output power achieved corresponded to the SA with $\alpha'_{SA} = 2\%$. It was 131 mW at 2063.6 nm with a slope efficiency of 11%. The laser threshold was at ~0.7 W of absorbed pump power, and the optical-to-optical efficiency was ~7%. The Q-switching conversion efficiency with respect to the CW regime was then 58%. For $\alpha'_{SA} = 3.5\%$, we extracted 85 mW at 2061.1 nm with a reduced slope $\eta = 6\%$. This is attributed to higher upconversion loss due to lower T_{SA}. The Q-switching conversion efficiency was only 38%.

The laser spectra of the PQS Tm,Ho:KLuW microchip laser are shown in Fig. 4(a). The spectra consisted only of a single emission peak. These laser wavelengths are in agreement with the maxima in the gain cross-section spectrum of Ho^{3+} ions in KLuW; see Fig. 4(b). For light polarization $E\|N_m$, the gain spectrum exhibits two local maxima centered at ~2060 and 2076 nm. For high inversion ratios ($\beta > 0.25$) associated with high T_{OC} and small T_{SA}, the laser is expected to oscillate near the short-wavelength peak at ~2060 nm.

By increasing the pump power, the duration of the single Q-switched pulse (FWHM) decreased only slightly from 16 to 14 ns ($\alpha'_{SA} = 2\%$) and from ~11 to 9 ns ($\alpha'_{SA} = 3.5\%$). This reduction was accompanied by a near-linear increase in the pulse repetition frequency (PRF), from 4.5 to 14.5 kHz ($\alpha'_{SA} = 2\%$) and from 3 to 8.2 kHz ($\alpha'_{SA} = 3.5\%$); see Fig. 5. By using the data on the average output power, PRF, and pulse duration, we calculated the pulse energies ($E_{out} = P_{out}/\mathrm{PRF}$) and peak powers ($P_{peak} = E_{out}/\Delta t$) for the studied PQS Tm,Ho:KLuW microchip laser; see Fig. 6. For both SAs, the pulse energy was nearly independent of the pump level, 9.0 ± 0.2 μJ ($\alpha'_{SA} = 2\%$) and 10.2 ± 0.3 μJ ($\alpha'_{SA} = 3.5\%$), and the maximum peak power amounted to 0.65 and 1.15 kW, respectively. The use of a SA with $\alpha'_{SA} = 3.5\%$ was superior with respect to the pulse duration and energy mainly due to an increased modulation depth.

The criterion for efficient passive Q-switching by a slow SA is [31]

$$X = \frac{\sigma_{gs}}{\sigma^g_{abs} + \sigma^g_{SE}} \frac{A_g}{A_{SA}} \gg 1. \quad (3)$$

For the Tm,Ho:KLuW microchip laser, the sizes of the laser mode in the active medium and in the SA are nearly the same ($A_g \approx A_{SA}$), so that the value of X is determined solely by the spectroscopic parameters of the Tm,Ho:KLuW and Cr:ZnS

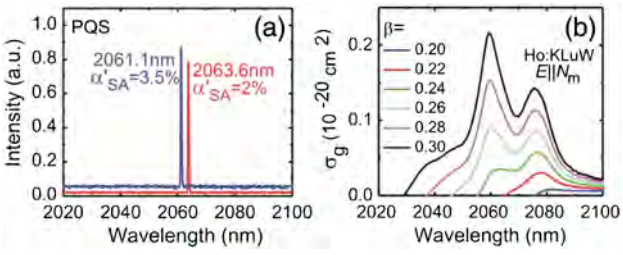

Fig. 4. (a) Typical laser emission spectra of the passively Q-switched Tm,Ho:KLuW microchip laser. (b) Gain cross sections, σ_g, of the Ho^{3+} ions in KLuW for light polarization $E\|N_m$; β, inversion ratio.

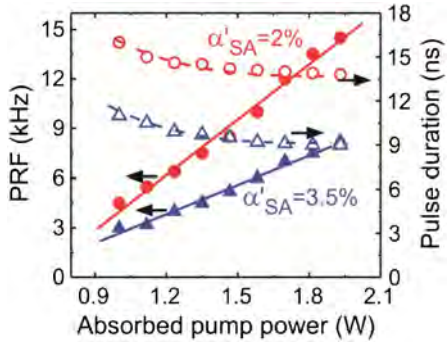

Fig. 5. Pulse duration and pulse repetition frequency for the passively Q-switched Tm,Ho:KLuW microchip laser.

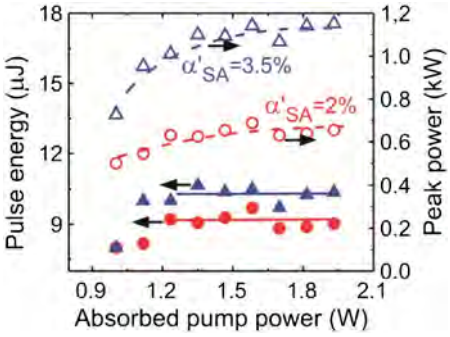

Fig. 6. Pulse energy and peak power for the passively Q-switched Tm,Ho:KLuW microchip laser.

materials. For a laser wavelength of ~2.06 μm, X is ~3 which means that although this combination of materials facilitates efficient Q-switching, the pulse energy and duration may show slight dependence on the pump power with saturation well above the laser threshold; see Figs. 5 and 6. The experimental values of pulse duration and energy agree well with the theoretical predictions for $T_{OC} = 5\%$; see Fig. 2. For $\alpha'_{SA} = 4\%$ and 2%, the model predicted generation of 9.8 ns/11 μJ and 13.6 ns/8.4 μJ pulses which correlates well with Figs. 5 and 6.

No damage of the Cr:ZnS SA was observed in our experiments. Indeed, the maximum axial peak intensity on the SA, $I_{in} = X[2E_{out}/\pi w_l^2 \Delta t]$ (where $X = (1 + R)/(1 - R)$ and R is the reflectivity of the OC, w_l is the radius of the laser mode, and the term "2" indicates that it has a Gaussian spatial profile corresponding to a TEM_{00} mode) was ~0.5 GW/cm^2 ($\alpha'_{SA} = 2\%$) and 0.8 GW/cm^2 ($\alpha'_{SA} = 3.5\%$), which is well below its damage threshold (>10 GW/cm^2 for picosecond-long pulses [32]).

Figure 7 shows the oscilloscope traces of the shortest Q-switched pulses for $\alpha'_{SA} = 2\%$ and 3.5% and a typical pulse train for $\alpha'_{SA} = 2\%$ (in all cases, $P_{abs} = 1.9$ W). The intensity instabilities in the pulse train are ~15% . They are attributed to the heating of the SA by the residual nonabsorbed pump.

The output beam of the Tm,Ho:KLuW microchip laser corresponded to a TEM_{00} mode with an almost circular profile and $M^2_{x,y} < 1.1$ ($x \equiv p$, $y \equiv m$), as can be expected from the very low astigmatism of the thermal lens ($S/M = 4\%$) [15] and the symmetrical four-side cooling of the laser crystal.

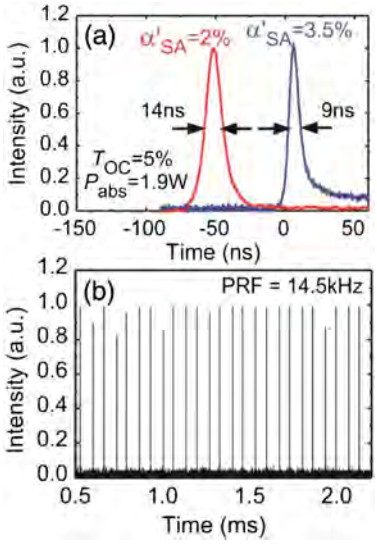

Fig. 7. (a) Records of the shortest laser pulses achieved with $\alpha'_{SA} = 2\%$ and 3.5%, and (b) a typical pulse train for the Tm,Ho:KLuW microchip laser Q-switched with Cr^{2+}:ZnS SA; $\alpha'_{SA} = 2\%$, $T_{OC} = 5\%$, and $P_{abs} = 1.9$ W.

So far, active and passive Q-switching of Tm,Ho bulk lasers have been intensively studied. Because Tm,Ho-codoped materials suffer from strong upconversion losses limiting their output performance, previous studies with active Q-switching were mainly performed with cryogenic cooling of the active material (typically at liquid nitrogen temperature, 77 K). By using an acousto-optic modulator (AOM) or a RTP Pockels cell, PQS Tm, Ho:YVO_4, $GdVO_4$, $LiYF_4$, and $YAlO_3$ lasers have been demonstrated generating typically 1–2 mJ/20 ns pulses with a multiwatt-level output [33–36]. Room-temperature AOM Q-switched Tm,Ho:YLF lasers were also reported, however, with much worse output characteristics [37]. Passive Q-switched laser operation at room temperature is more favorable to benefit from the compactness of the cavity. A comparison of passively Q-switched Tm,Ho bulk lasers reported so far [19–23] is presented in Table 2. Two types of SAs were employed in these lasers, namely, Cr:ZnS and carbon nanostructures (graphene and single-walled carbon nanotubes, SWCNTs). However, they provided similar output characteristics with a pulse duration of hundreds of ns and a pulse energy of a few microjoules. Although the results in the present work do not present any record in terms of average output power or pulse energy, they represent a substantial reduction in the pulse duration and, consequently, a few orders of magnitude increase in the peak power, from a few W to the ~1 kW level.

Further improvement of the developed laser can be expected by decreasing the intracavity losses, i.e., applying AR-coatings on the laser crystal or improving the ratio of the saturable to the nonsaturable SA losses. The use of Cr:ZnSe, which demonstrates a higher ground-state absorption cross section at the Ho^{3+} laser wavelength ($\sigma_{gs} = 2.5 \times 10^{-18}$ cm^2 at ~2.06 μm) as compared with its Cr:ZnS counterpart [38], seems to be useful for increasing the modulation depth of the SA which is important for obtaining shorter duration and higher energy pulses. In this way, according to our model, the generation of peak powers up to ~10 kW from a room-temperature Tm,Ho:KLuW microchip laser is expected.

5. CONCLUSIONS

We report on the first, to the best of our knowledge, passively Q-switched Tm,Ho-codoped double tungstate microchip laser using polycrystalline Cr^{2+}:ZnS as saturable absorber and a 5 at. % Tm, 0.5 at.% Ho:KLuW crystal cut along the N_g-axis as the gain medium. This laser generated a maximum average output power of 131 mW at 2063.6 nm with a slope efficiency of 11% ($\alpha'_{SA} = 2\%$). With higher modulation depth of the SA ($\alpha'_{SA} = 3.5\%$), a pulse duration of 9 ns was achieved, the shortest ever reported for a PQS Tm,Ho-doped laser. At a pulse energy of 10.4 μJ, this corresponds to a record peak power of 1.15 kW, the highest ever extracted from a room-temperature PQS Tm,Ho laser, exceeding >50 times the previous results [19–23]. A theoretical model of a quasi-three-level laser system PQS with a "slow" SA is developed. It agrees well with the experimental results. Further improvement of the output characteristics of the compact ~2 μm Tm,Ho PQS room-temperature microchip can be expected by use of Cr:ZnSe SA and optimization of intracavity losses.

APPENDIX A

Solutions of Eq. (1) for the photon flux density at laser frequency (Φ_g), effective population of the upper laser level at the moments when Φ_g reaches its maximum value (N^t_{2g}), and the termination of the laser pulse (N^f_{2g}) are given by

$$\Phi_g(N_{2g}) = \frac{c\mu}{n}\left\{\begin{array}{l} N^i_{2g} - N_{2g} - \frac{k_L l_{AM} + \beta \ln(1/T_{SA})}{l_{AM}\sigma_g} \ln\left(\frac{N^i_{2g}}{N_{2g}}\right) - \\ - \frac{(1-\beta)\ln(1/T_{SA})}{l_{AM}\sigma_g \alpha}\left[1 - \left(\frac{N^i_{2g}}{N_{2g}}\right)^{\alpha}\right] \end{array}\right\}, \quad \text{(A1)}$$

Table 2. Summary of PQS Near-Room-Temperature Tm,Ho Lasers Reported So Far

Crystal, Tm,Ho:	SA	P_{out}, mW	Δt, Ns	PRF, kHz	E_{out}, μJ	P_{peak}, kW	T, K	Ref.
KLuW	A	85	9	8.2	10.4	1.15	287	This work
	A	131	14	14.5	9	0.65	287	
KLuW	B	74	200	340	0.2	0.001	285	[19]
$LiYF_4$	A	10	1250	2.6	4	0.003	283	[20]
$LiLuF_4$	A	68	1200	5.2	13	0.01	283	[21]
$YAlO_3$	C	660	135	245	2.7	0.02	285	[23]

P_{out}, average output power; Δt, pulse duration; E_{out}, pulse energy; PRF, pulse repetition frequency; P_{peak}, peak power.

SA: A—Cr:ZnS, B—graphene, C—SWCNTs.

$$\frac{N_{2g}^{t}}{N_{2g}^{i}} = \frac{N_{2g}^{\circ}}{N_{2g}^{i}} + \left(1 - \frac{N_{2g}^{\circ}}{N_{2g}^{i}}\right)\left(\frac{N_{2g}^{t}}{N_{2g}^{i}}\right)^{\alpha}, \quad \textbf{(A2)}$$

$$\frac{N_{2g}^{f}}{N_{2g}^{i}} = 1 + \frac{N_{2g}^{0}}{N_{2g}^{i}} \ln\left(\frac{N_{2g}^{f}}{N_{2g}^{i}}\right) - \frac{1}{\alpha}\left(1 - \frac{N_{2g}^{0}}{N_{2g}^{i}}\right)\left[1 - \left(\frac{N_{2g}^{t}}{N_{2g}^{i}}\right)^{\alpha}\right], \quad \textbf{(A3)}$$

where $\alpha = \xi\sigma_{gs}/\sigma_{g}$, $\beta = \sigma_{es}/\sigma_{gs}$, and $N_{2g}^{0} = (k_L l_{\mathrm{AM}} - \beta \ln T_{\mathrm{SA}})/(\sigma_g l_{\mathrm{AM}})$.

Funding. Spanish Government (MAT2013-47395-C4-4-R, TEC2014-55948-R); Generalitat de Catalunya (2014SGR1358); ICREA Academia for Excellence in Research (2010ICREA-02); European Commission: Marie Skłodowska-Curie (657630).

REFERENCES

1. P. A. Budni, L. A. Pomeranz, M. L. Lemons, C. A. Miller, J. R. Mosto, and E. P. Chicklis, "Efficient mid-infrared laser using 1.9-μm-pumped Ho:YAG and $ZnGeP_2$ optical parametric oscillators," J. Opt. Soc. Am. B **17**, 723–728 (2000).
2. T. Y. Fan, G. Huber, R. L. Byer, and P. Mitzscherlich, "Spectroscopy and diode laser-pumped operation of Tm, Ho:YAG," IEEE J. Quantum Electron. **24**, 924–933 (1988).
3. B. M. Walsh, N. P. Barnes, and B. Di Bartolo, "On the distribution of energy between the Tm $^3F_4$ and Ho $^5I_7$ manifolds in Tm-sensitized Ho luminescence," J. Lumin. **75**, 89–98 (1997).
4. T. Y. Fan, G. Huber, R. L. Byer, and P. Mitzscherlich, "Continuous-wave operation at 2.1 μm of a diode-laser-pumped, Tm-sensitized Ho:$Y_3Al_5O_{12}$ laser at 300 K," Opt. Lett. **12**, 678–680 (1987).
5. I. F. Elder and M. J. P. Payne, "Lasing in diode-pumped Tm:YAP, Tm, Ho:YAP and Tm, Ho:YLF," Opt. Commun. **145**, 329–339 (1998).
6. P. J. Morris, W. Lüthy, H. P. Weber, Y. D. Zavartsev, P. A. Studenikin, I. Shcherbakov, and A. I. Zagumenyi, "Laser operation and spectroscopy of Tm: Ho: $GdVO_4$," Opt. Commun. **111**, 493–496 (1994).
7. J. J. Zayhowski, "Microchip lasers," Opt. Mater. **11**, 255–267 (1999).
8. G. L. Bourdet and G. Lescroart, "Theoretical modeling and design of a Tm, Ho:$YLiF_4$ microchip laser," Appl. Opt. **38**, 3275–3281 (1999).
9. J. Izawa, H. Nakajima, H. Hara, and Y. Arimoto, "A tunable and longitudinal mode oscillation of a Tm, Ho:YLF microchip laser using an external etalon," Opt. Commun. **180**, 137–140 (2000).
10. B. Q. Yao, F. Chen, P. B. Meng, C. H. Zhang, and Y. Z. Wang, "Diode pumped operation of Tm, Ho:YAP microchip laser," Laser Phys. **21**, 674–676 (2011).
11. B. Q. Yao, F. Chen, C. T. Wu, Q. Wang, G. Li, C. H. Zhang, Y. Z. Wang, and Y. L. Ju, "Diode-end-pumped Tm, Ho:YVO_4 microchip laser at room temperature," Laser Phys. **21**, 663–666 (2011).
12. R. L. Zhou, Y. L. Ju, C. T. Wu, Z. G. Wang, and Y. Z. Wang, "A single-longitudinal-mode CW 0.25 mm Tm, Ho:$GdVO_4$ microchip laser," Laser Phys. **20**, 1320–1323 (2010).
13. V. Petrov, M. C. Pujol, X. Mateos, O. Silvestre, S. Rivier, M. Aguilo, R. Sole, J. Liu, U. Griebner, and F. Diaz, "Growth and properties of $KLu(WO_4)_2$, and novel ytterbium and thulium lasers based on this monoclinic crystalline host," Laser Photon. Rev. **1**, 179–212 (2007).
14. V. Jambunathan, A. Schmidt, X. Mateos, M. C. Pujol, U. Griebner, V. Petrov, C. Zaldo, M. Aguiló, and F. Díaz, "Crystal growth, optical spectroscopy, and continuous-wave laser operation of co-doped (Ho, Tm):$KLu(WO_4)_2$ monoclinic crystals," J. Opt. Soc. Am. B **31**, 1415–1421 (2014).
15. P. Loiko, J. M. Serres, X. Mateos, K. Yumashev, N. Kuleshov, V. Petrov, U. Griebner, M. Aguiló, and F. Díaz, "Microchip laser operation of Tm, Ho:$KLu(WO_4)_2$ crystal," Opt. Express **22**, 27976–27984 (2014).
16. J. J. Zayhowski and C. Dill, "Diode-pumped passively *Q*-switched picosecond microchip lasers," Opt. Lett. **19**, 1427–1429 (1994).
17. J. Dong, K. Ueda, A. Shirakawa, H. Yagi, T. Yanagitani, and A. A. Kaminskii, "Composite Yb:YAG/Cr^{4+}:YAG ceramics picosecond microchip lasers," Opt. Express **15**, 14516–14523 (2007).
18. J. M. Serres, X. Mateos, P. Loiko, K. Yumashev, N. Kuleshov, V. Petrov, U. Griebner, M. Aguiló, and F. Díaz, "Diode-pumped microchip Tm:$KLu(WO_4)_2$ laser with more than 3 W of output power," Opt. Lett. **39**, 4247–4250 (2014).
19. J. M. Serres, P. Loiko, X. Mateos, V. Jambunathan, K. Yumashev, U. Griebner, V. Petrov, M. Aguiló, and F. Díaz, "*Q*-switching of a Tm, Ho:$KLu(WO_4)_2$ microchip laser by a graphene-based saturable absorber," Laser Phys. Lett. **13**, 025801 (2016).
20. X. Zhang, X. Bao, L. Li, H. Li, and J. Cui, "Laser diode end-pumped passively *Q*-switched Tm, Ho:YLF laser with Cr:ZnS as a saturable absorber," Opt. Commun. **285**, 2122–2127 (2012).
21. X. Zhang, L. Yu, S. Zhang, L. Li, J. Zhao, and J. Cui, "Diode-pumped continuous wave and passively *Q*-switched Tm, Ho:LLF laser at 2 μm," Opt. Express **21**, 12629–12634 (2013).
22. Y.-Q. Du, B.-Q. Yao, Z. Cui, X.-M. Duan, T.-Y. Dai, Y.-L. Ju, Y.-B. Pan, M. Chen, and Z.-C. Shen, "Passively *Q*-switched Tm, Ho:YVO_4 laser with Cr:ZnS saturable absorber at 2 μm," Chin. Phys. Lett. **31**, 064209 (2014).
23. T. L. Feng, S. Z. Zhao, K. J. Yang, G. Q. Li, D. C. Li, J. Zhao, W. C. Qiao, L. H. Zheng, J. Xu, G. J. Zhao, and Y. G. Wang, "A diode-pumped passively *Q*-switched Tm, Ho:YAP laser with a single-walled carbon nanotube," Laser Phys. Lett. **10**, 095001 (2013).
24. M. Segura, M. Kadankov, X. Mateos, M. C. Pujol, J. J. Carvajal, M. Aguiló, F. Díaz, U. Griebner, and V. Petrov, "Passive *Q*-switching of the diode pumped Tm^{3+}: $KLu(WO_4)_2$ laser near 2-μm with Cr^{2+}: ZnS saturable absorbers," Opt. Express **20**, 3394–3400 (2012).
25. P. Loiko, J. M. Serres, X. Mateos, K. Yumashev, A. Yasukevich, V. Petrov, U. Griebner, M. Aguiló, and F. Díaz, "Subnanosecond Tm:KLuW microchip laser *Q*-switched by a Cr:ZnS saturable absorber," Opt. Lett. **40**, 5220–5223 (2015).
26. V. Jambunathan, A. Schmidt, X. Mateos, M. C. Pujol, J. J. Carvajal, M. Aguiló, F. Díaz, U. Griebner, and V. Petrov, "Continuous-wave co-lasing in a monoclinic co-doped (Ho, Tm): $KLu(WO_4)_2$ crystal," Laser Phys. Lett. **8**, 799–803 (2011).
27. P. A. Loiko, J. M. Serres, X. Mateos, K. V. Yumashev, N. V. Kuleshov, V. Petrov, U. Griebner, M. Aguiló, and F. Díaz, "Characterization of thermal lens in Tm:$KLu(WO_4)_2$ and microchip laser operation," Laser Phys. Lett. **11**, 075001 (2014).
28. P. Loiko, F. Druon, P. Georges, B. Viana, and K. Yumashev, "Thermo-optic characterization of Yb:$CaGdAlO_4$ laser crystal," Opt. Mater. Express **4**, 2241–2249 (2014).
29. V. E. Kisel, A. S. Yasukevich, N. V. Kondratyuk, and N. V. Kuleshov, "Diode-pumped passively *Q*-switched high-repetition-rate Yb microchip laser," Quantum Electron. **39**, 1018–1022 (2009).
30. I. T. Sorokina, E. Sorokin, S. Mirov, V. Fedorov, V. Badikov, V. Panyutin, A. di Lieto, and M. Tonelli, "Continuous-wave tunable Cr^{2+}:ZnS laser," Appl. Phys. B **74**, 607–611 (2002).
31. A. E. Siegman, *Lasers* (University Science Books, 1986), pp. 1024–1028.
32. D. M. Simanovskii, H. A. Schwettman, H. Lee, and A. J. Welch, "Midinfrared optical breakdown in transparent dielectrics," Phys. Rev. Lett. **91**, 107601 (2003).
33. B. Q. Yao, Y. Z. Wang, Y. L. Ju, and W. J. He, "Performance of AO *Q*-switched Tm, Ho: $GdVO_4$ laser pumped by a 794 nm laser diode," Opt. Express **13**, 5157–5162 (2005).
34. B. Q. Yao, G. Li, P. B. Meng, G. L. Zhu, Y. L. Ju, and Y. Z. Wang, "High power diode-pumped continuous wave and *Q*-switch operation of Tm, Ho:YVO_4 laser," Laser Phys. Lett. **7**, 857–861 (2010).
35. L. J. Li, B. Q. Yao, C. W. Song, Y. Z. Wang, and Z. G. Wang, "Continuous wave and AO *Q*-switch operation Tm, Ho:YAP laser pumped by a laser diode of 798 nm," Laser Phys. Lett. **6**, 102–104 (2009).

36. P. B. Meng, B. Q. Yao, G. L. Zhu, Y. L. Ju, and Y. Z. Wang, "RTP Q-switched 2 μm Tm, Ho:$GdVO_4$ laser," Laser Phys. Lett. **21**, 94–96 (2011).
37. B. T. McGuckin, R. T. Menzies, and H. Hemmati, "Efficient energy extraction from a diode pumped Q-switched Tm, Ho:$YLiF_4$ laser," Appl. Phys. Lett. **59**, 2926–2928 (1991).
38. A. V. Podlipensky, V. G. Shcherbitsky, N. V. Kuleshov, V. P. Mikhailov, V. I. Levchenko, and V. N. Yakimovich, "Cr^{2+}:ZnSe and Co^{2+}:ZnSe saturable-absorber Q-switches for 1.54-μm Er:glass lasers," Opt. Lett. **24**, 960–962 (1999).